Mixing properties of steady flow in thermocapillary driven droplets

Dmitri L. Vainchtein
School of Physics, Georgia Institute of Technology, Atlanta, Georgia 30332 and Space Research Institute, ul. Profsouznaya, 84/32, GSP-7, 117997 Moscow, Russia

John Widloski and Roman O. Grigoriev
School of Physics, Georgia Institute of Technology, Atlanta, Georgia 30332

(Received 1 September 2006; accepted 10 April 2007; published online 12 June 2007)

We consider mixing via chaotic advection in microdroplets suspended at the free surface of a liquid substrate and driven along a straight line using the thermocapillary effect. With the help of a model derived by Grigoriev [Phys. Fluids **17**, 033601 (2005)] we show that the mixing properties of the flow inside the droplet can vary dramatically as a function of the physical properties of the fluids and the imposed temperature profile. Proper characterization of the mixing quality requires introduction of two different metrics. The first metric determines the relative volumes of the domain of chaotic streamlines and the domain of regular streamlines. The second metric describes the time for homogenization inside the chaotic domain. We compute both metrics using perturbation theory in the limit of weak temperature dependence of the surface tension coefficient at the free surface of the substrate. © *2007 American Institute of Physics*. [DOI: 10.1063/1.2738846]

I. INTRODUCTION

Mixing in small discrete volumes of fluid via chaotic advection represents a problem of considerable practical interest. For instance, many applications of microfluidics require thorough blending of various samples. However, the length and velocity scales of the flow in typical microfluidic devices are such that turbulence, which is mostly responsible for mixing at large scales, does not arise, while the molecular diffusion, which acts at the small scales, is too slow. The challenge is therefore to find effective ways to mix the fluid using advection by a laminar flow. This problem has been studied theoretically and experimentally in the context of liquid droplets driven by pressure gradients[1–3] and electric fields.[4,5] An alternative physical implementation involves microdroplets suspended at the free surface of a liquid substrate and driven using the thermocapillary effect.[6,7] In all of these studies the bulk of attention was devoted to time-periodic flows often found to possess rather good mixing properties.

In this paper we consider mixing in thermocapillary driven microdroplets moving with a constant speed in a straight line along the substrate surface, which results in a steady flow. Experiments found the mixing to be very poor in this regime.[7] However, a numerical study of the simplified model of the flow constructed in Ref. 6 shows that the mixing efficiency can be improved dramatically by appropriately choosing the parameters such as the magnitude of the temperature coefficients of surface tension at different fluid interfaces, the ratio $\lambda=\mu_{\text{in}}/\mu_{\text{out}}$ of the fluid viscosities inside and outside the droplet, and the curvature of the temperature field driving the flow.

Our objective is to quantitatively describe the mixing properties of the flow as a function of parameters—that is, how thorough and quick the mixing process is—with the goal to provide further guidance to experiments. To that end, we start in Sec. II by describing the theoretical model of the flow inside thermocapillary driven droplets. A perturbative analysis of the mixing process (in the limit of small temperature coefficient of surface tension at the free surface of the liquid substrate) using the method of averaging is presented in Sec. III. Finally, our conclusions and the topics for future study are presented in Sec. IV.

II. THE MODEL

In the situations of most interest, where the droplet size is on the order of a few microns to a few millimeters, the flow is characterized by a small Reynolds number and can be found by solving the quasistatic Stokes equation subject to the boundary conditions reflecting the physical nature of the driving field. Due to the linearity of the Stokes equation, the corresponding solutions can be constructed using a linear superposition of simple bounded component flows.

To simplify the mathematical description of the problem, we will follow Ref. 6, assuming that the droplet is suspended below the free surface of the liquid substrate rather than at its surface, and consider the limit of small capillary numbers such that the droplet can be considered spherical. Under these assumptions, a superposition of three components flows, with appropriate magnitude and orientation, is needed to describe the interior flow to leading order. In nondimensional units (with distances scaled by the droplet radius and the origin located at the center of the drop), these three component flows are the dipole flow $\mathbf{v}_d$,

$$\begin{aligned} \dot{x}_d &= 1 + x^2 - 2r^2, \\ \dot{y}_d &= xy, \\ \dot{z}_d &= xz, \end{aligned} \tag{1}$$

the quadrupole flow $\mathbf{v}_q$,

$$\dot{x}_q = 2x(1 + x^2 - 2r^2),$$

$$\dot{y}_q = y(r^2 + 2x^2 - 1), \tag{2}$$

$$\dot{z}_q = z(r^2 + 2x^2 - 1),$$

and the Taylor flow $\mathbf{v}_t$,

$$\dot{x}_t = z(\beta(5r^2 - 3 - 4x^2) + 2),$$

$$\dot{y}_t = -4\beta xyz, \tag{3}$$

$$\dot{z}_t = x(\beta(5r^2 - 3 - 4z^2) - 2),$$

where $r^2 = x^2 + y^2 + z^2$, $\beta = 1/(1+\lambda)$ (the value $\beta = 0.5$ is used in all numerical calculations throughout the paper), the x axis points in the direction of the thermal gradient, and the z axis is vertical. The components $\mathbf{v}_d$ and $\mathbf{v}_q$ are caused by the thermocapillary effect at the droplet surface, while $\mathbf{v}_t$ arises due to the thermocapillary effect at the surface of the liquid substrate.

The complete flow inside the droplet can be written as a linear superposition of the dipole, Taylor, and quadrupole flows

$$\mathbf{v} = \mathbf{v}_d + \varepsilon \mathbf{v}_t + q\mathbf{v}_q. \tag{4}$$

The parameters ε and q determine the relative strengths of the three components which depend on the temperature coefficients of surface tension at the droplet surface and the free surface of the substrate fluid and on the nonuniformity of the imposed temperature gradient.[6] As the dipole component is present in almost any setting, it is convenient to set its magnitude to unity by an appropriate choice of the time scale.

Three component flows (1)–(3) and complete flow (4) are volume-preserving and bounded by the droplet surface $r=1$, which represents an invariant set. Moreover, the plane $y=0$ is an invariant set for each flow. Since the flow for $y<0$ is a mirror image of the flow for $y>0$ and there is no transport across the $y=0$ plane, we will restrict our attention to the flow inside the hemisphere characterized by positive values of y.

All component flows (1)–(3) are integrable, and each has a pair of invariants. These are

$$I_d = z/y, \quad J_d = z^2(1 - r^2) \tag{5}$$

for the dipole flow,

$$I_q = z/y, \quad J_q = xz^2(1 - r^2) \tag{6}$$

for the quadrupole flow, and

$$I_t = y^3(1 - r^2), \quad J_t = y(1 - r^2)(1 + \beta(z^2 - x^2)) \tag{7}$$

for the Taylor flow. Each component, taken in isolation, generates closed streamlines confined to an intersection of level sets of the two invariants and, as a consequence, has extremely poor mixing qualities.

An arbitrary linear superposition of the dipole and quadrupole components [i.e., (4) with $\varepsilon=0$] is again integrable and possesses two invariants:

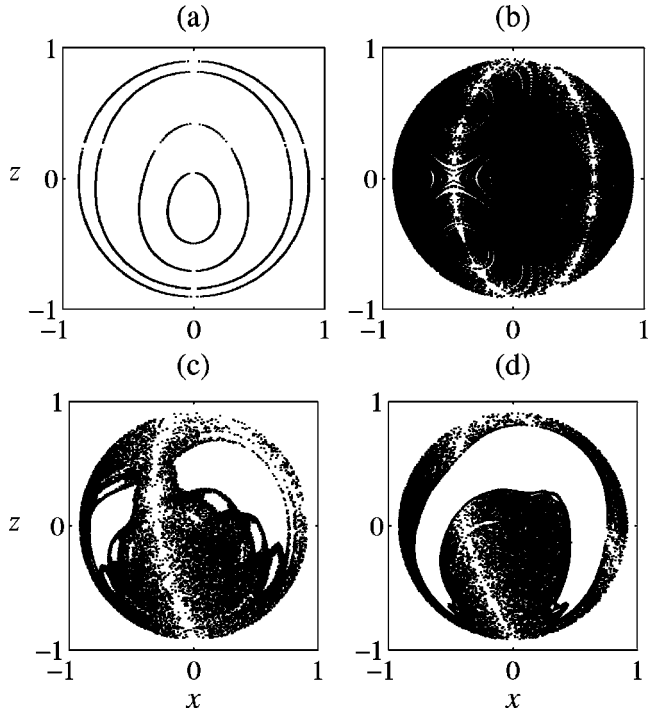

FIG. 1. Characteristic Poincaré sections of flow (4): (a) $q=-0.01$, $\varepsilon=2$ (regular regime), (b) $q=-2$, $\varepsilon=0.01$ (chaotic regime), (c) $q=-0.75$, $\varepsilon=0.75$ (mixed regular/chaotic regime), (d) $q=-1$, $\varepsilon=1$ (mixed regular/chaotic regime). Panel (a) shows two different streamlines, panels (b)–(d) each show one streamline. On all the panels $\beta=0.5$.

$$I_{d+q} = z/y, \quad J_{d+q} = y^2(1 + 2qx)(1 - r^2). \tag{8}$$

A linear superposition of the dipole and Taylor components [i.e., (4) with $q=0$] is also integrable and possesses two invariants which, for $\beta=0$, are given by

$$I_{d+t} = (2\varepsilon - z)/y, \quad J_{d+t} = y^2(1 - r^2). \tag{9}$$

The existence of invariants is a consequence of the fact that, in both cases, the component flows have a mutual symmetry[6] (axial symmetry with respect to the x axis for dipole-quadrupole flow and a mirror symmetry with respect to the $x=0$ plane for the dipole-Taylor flow).

A linear superposition of the quadrupole and Taylor components, on the other hand, has no invariants—the two components have no mutual symmetries aside from the mirror symmetry with respect to the $y=0$ plane common to all three component flows. As a consequence, the quadrupole-Taylor flow is, in general, chaotic. This result, however, has little practical significance as, in the model of thermocapillary driven droplets, the Taylor flow vanishes when the dipole flow vanishes. We, therefore, come to a conclusion that all three components are needed to achieve mixing in three dimensions.

To illustrate the mixing properties of complete three-component flow (4), we numerically integrate the evolution equations starting from a generic initial condition. Sample results are presented in Fig. 1 for different strengths ε of the Taylor component and q of the quadrupole component. As the characteristic Poincaré sections of the flow (by the $y=0.4$ plane) show, the volume fraction of the chaotic domain

varies from nearly 0% for $q=-0.01$, $\varepsilon=2.0$ [see Fig. 1(a)], indicating that essentially all streamlines remain nonchaotic, to almost 100% for $q=-2.0$, $\varepsilon=0.01$ [see Fig. 1(b)], when essentially all streamlines become chaotic. Figures 1(c) and 1(d) illustrate the mixing properties of the flow in the intermediate regime. Numerical simulations here and in the remainder of this paper were performed using the MATLAB implementation of the variable time step fourth to fifth order Runge-Kutta scheme. Although a custom volume-preserving integrator could, in principle, be more efficient, we found that accurate results, even for relatively long integration times used here, could be achieved by simply increasing the tolerance of the nonvolume-preserving Runge-Kutta integrator.

It is clear that if a similar flow were to be used in an experiment to homogenize the droplet interior, the parameters should be chosen in the chaotic regime. In order to understand the dependence of the mixing properties of the three-component flow on the parameters, we will restrict our attention to the case of small values of ε [in other words, we will assume $|q|=O(1)$ and $0\leqslant\varepsilon\ll 1$]. This will allow us to describe the mixing process quantitatively using perturbation theory.[8]

III. THE LIMIT OF WEAK TAYLOR COMPONENT

In this section we describe the gradual destruction of flow invariants of (4) as ε is increased from zero. Since invariant surfaces (level sets of the invariants) serve as transport barriers (see, e.g., Ref. 6), we will find that the mixing properties of the flow become progressively better as the invariants disintegrate.

A. Unperturbed system

For $\varepsilon=0$, flow (4) reduces to a superposition of the dipole and quadrupole flows and possesses two invariants (8). An alternative (equivalent, but more convenient) set of invariants is the azimuthal angle φ (around the x axis) and the stream function ψ,

$$\varphi=\arctan(z/y),$$
$$\psi=\tfrac{1}{2}(1+2qx)\rho^2(1-r^2), \tag{10}$$

where we have defined $\rho^2=y^2+z^2$.

The flow structure of the unperturbed system depends on the value of q. Note that the dynamics for $q>0$ is the same as for $q<0$ up to the reflection with respect to the plane $x=0$. For all values of q there is a pair of hyperbolic fixed points at the poles $x=\pm 1$, $\rho=0$ and a circle of degenerate elliptic fixed points at

$$x_{\rm ell}^{-}=\frac{-1+\sqrt{1+5q^2}}{5q},\quad \rho_{\rm ell}^{-}=\sqrt{\frac{1-(x_{\rm ell}^{-})^2}{2}}, \tag{11}$$

corresponding to the maximum of ψ. For $|q|>0.5$, another circle of degenerate elliptic fixed points appears at

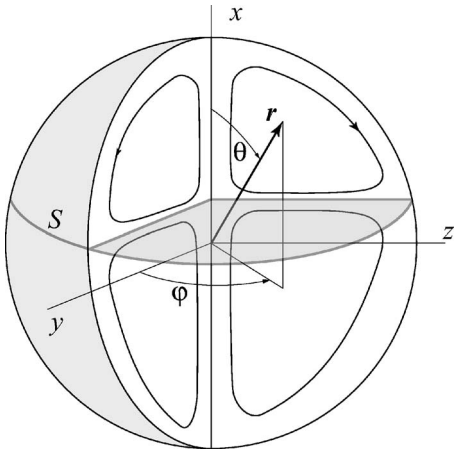

FIG. 2. A sketch of the unperturbed flow for $|q|>0.5$.

$$x_{\rm ell}^{+}=\frac{-1-\sqrt{1+5q^2}}{5q},\quad \rho_{\rm ell}^{+}=\sqrt{\frac{1-(x_{\rm ell}^{+})^2}{2}}, \tag{12}$$

corresponding to the minimum of ψ, accompanied by a hyperbolic fixed point $x=x_s\equiv -1/(2q)$, $\rho=0$ and a circle of degenerate hyperbolic fixed points on the surface at $x=x_s$, $r=1$. The plane $x=x_s$ (denoted S below) is a separatrix (see Fig. 2).

Each streamline $\Gamma_{\psi,\varphi}$ of the flow lies at the intersection of the plane $\varphi=$const with the axisymmetric surface $\psi=$const, the x axis is the axis of symmetry. All streamlines, except for those passing through the fixed points, are closed curves. A point inside the sphere that does not lie on S or on the x axis can be specified by the coordinates ψ, φ, and s. Here $s(\mathrm{mod}\ 2\pi)$ is a uniform phase along $\Gamma_{\psi,\varphi}$ such that $\dot{s}=\Omega(\psi)$ [where $\Omega(\psi)$ is the angular frequency of the unperturbed system] and $s=0$ at the point closest to the surface.

B. Weakly perturbed system

For $0<|\varepsilon|\ll 1$, essentially all streamlines do not close after one turn (corresponding to $\Delta s\approx 2\pi$), as the values of φ and ψ start to drift,

$$\dot{\psi}=\varepsilon(q\rho^2(\beta(5r^2-3-4x^2)+2)+(1+2qx)x(\beta(2\rho^2+5r^2-3)-2))z(1-r^2),$$
$$\dot{\varphi}=\varepsilon x\cos\varphi\frac{\beta(5r^2-3)-2}{\rho}. \tag{13}$$

In terms of ψ, φ, and s, system (4) has the following form:

$$\dot{\psi}=\varepsilon f(\psi,\varphi,s),$$
$$\dot{\varphi}=\varepsilon g(\psi,\varphi,s), \tag{14}$$
$$\dot{s}=\Omega(\psi)+\varepsilon h(\psi,\varphi,s).$$

The functions f, g, h are 2π periodic in s. The variable s is fast, and the variables ψ and φ are slow. A streamline of the exact system resembles a spiral with every coil nearly following a closed streamline of the unperturbed system with

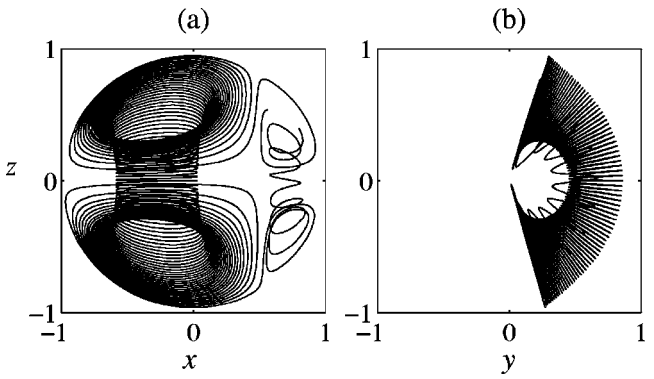

FIG. 3. A typical trajectory of the exact system computed for one period of averaged system (15). The parameters are $q=-1$ and $\varepsilon=10^{-2}$. The panels show the projections on the (x,z) and (y,z) planes.

the corresponding values of ψ and φ (see Fig. 3). Depending on the initial conditions, the resulting motion is either quasiperiodic (with streamlines confined to two-dimensional surfaces) or chaotic (with streamlines exploring all three dimensions).

The difference in characteristic time scales allows us to define the *averaged system*:

$$\dot{\psi} = \varepsilon F(\psi,\varphi),$$
$$\dot{\varphi} = \varepsilon G(\psi,\varphi), \tag{15}$$

where the functions F and G are the averages of f and g over one period of the unperturbed system,

$$F(\psi,\varphi) = \frac{1}{T(\psi)}\oint \frac{d\psi}{dt}dt = \frac{1}{T(\psi)}\oint (\nabla\psi\cdot\mathbf{v}_t)dt,$$
$$G(\psi,\varphi) = \frac{1}{T(\psi)}\oint \frac{d\varphi}{dt}dt = \frac{1}{T(\psi)}\oint (\nabla\varphi\cdot\mathbf{v}_t)dt. \tag{16}$$

Here the integrals are evaluated along $\Gamma_{\psi,\varphi}$ and $T(\psi)=2\pi/\Omega(\psi)$ is the period of the unperturbed motion along this streamline. Far from the separatrix [where $\Omega(\psi)\gg\varepsilon$], the solutions of the averaged system describe the behavior of ψ and φ along a streamline of the exact system to an accuracy of order ε over time intervals of order $1/\varepsilon$ (see Refs. 9 and 10).

Denoted by $\Phi(\psi,\varphi)$ the flux of the perturbation vector $\mathbf{v}_t$ across a surface Σ spanning the streamline of the unperturbed system, $\Gamma_{\psi,\varphi}=\partial\Sigma$. This flux depends on ψ and φ and is independent of the choice of the spanning surface, since the flow is incompressible. For example, one can choose a surface lying in the plane $\varphi=$const. Thus,

$$\Phi(\psi,\varphi) = \int_{\Sigma}(\mathbf{v}_t\cdot\mathbf{n})d\sigma, \tag{17}$$

where $\mathbf{n}$ and $d\sigma$ are the unit normal on Σ and an area element on Σ, respectively. The positive direction of $\mathbf{n}$ is taken to be the direction of the angular velocity of the unperturbed motion along $\Gamma_{\psi,\varphi}$. It was shown in Ref. 11 that

$$F(\psi,\varphi) = \frac{1}{T(\psi)}\frac{\partial\Phi(\psi,\varphi)}{\partial\varphi},$$
$$G(\psi,\varphi) = -\frac{1}{T(\psi)}\frac{\partial\Phi(\psi,\varphi)}{\partial\psi}. \tag{18}$$

Thus, the averaged system is Hamiltonian, with the Hamiltonian function $\varepsilon\Phi(\psi,\varphi)$. In particular, it follows that $\Phi(\psi,\varphi)$ is an invariant (or integral) of the averaged system and, hence, is an adiabatic invariant (AI) of the exact system.[8] Using the Stokes theorem, we can write Φ as an integral along $\partial\Sigma$,

$$\Phi(\psi,\varphi) = \oint_{\Gamma_{\psi,\varphi}}\mathbf{A}_t\cdot d\mathbf{l}, \tag{19}$$

where $d\mathbf{l}$ is the length element on $\Gamma_{\psi,\varphi}$ and $\mathbf{A}_t$ is a vector potential of the perturbation velocity field ($\mathbf{v}_t=\nabla\times\mathbf{A}_t$) given by

$$(A_x,A_y,A_z)_t = (1-r^2)(\beta xy,(1-\beta(x^2-z^2)),-\beta zy). \tag{20}$$

Substituting (20) into (19), we get

$$\Phi(\psi,\varphi) = \cos\varphi\oint_{\psi=\text{const}}(1-r^2)(\beta\rho x dx-(\beta x^2-1)d\rho), \tag{21}$$

where the integral is a function of ψ only. In simulations, an easy way to compute the value of Φ numerically is to take into account that $d\mathbf{l}=\mathbf{v}dt$, converting (19) into a time integral,

$$\Phi(\psi,\varphi) = \int_0^T \mathbf{A}_t\cdot(\mathbf{v}_d+q\mathbf{v}_q)dt. \tag{22}$$

Recall that the integration is done along an unperturbed streamline, so the term with $\mathbf{v}_t$ is absent.

Finally, it should be reiterated that averaged system (15) is a good approximation only as long as the streamline stays away from the separatrix. Far from the separatrix, during each turn of the fast system, the value of Φ oscillates with an amplitude of order ε. To quantify these oscillations of the exact streamline around the averaged one, we can consider *improved adiabatic invariants* (see, e.g., Ref. 8) that are conserved with the accuracy of order ε^2. Near the separatrix [where $\Omega(\psi)=O(\varepsilon)$] the averaging procedure breaks down. In particular, Φ can undergo arbitrarily big changes there. This phenomenon is discussed in more detail below.

C. Phase portrait of the averaged system

The structure of the phase portrait on the slow (φ,ψ) plane depends on the values of q. For $|q|<0.5$, there is no separatrix, so the averaging procedure is valid everywhere and hence the AI is constant, if one ignores small bounded oscillations with amplitude of order ε. Therefore, the entire drop is a regular domain: all streamlines reside on the tori that are levels sets of the AI.

For $|q|>0.5$, the separatrix $x=x_s=-1/(2q)$ in the physical space (or $\psi=0$ in the slow plane) appears inside the drop.

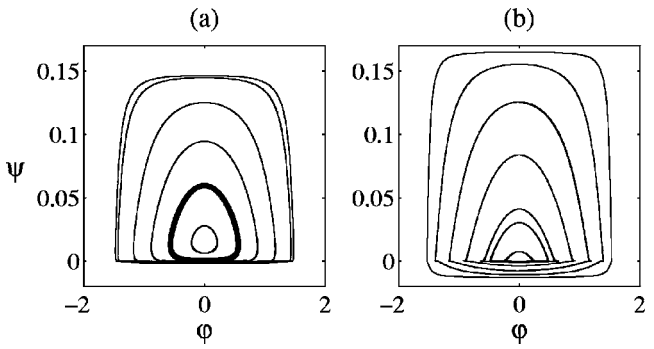

FIG. 4. Phase portraits of the averaged system on the (φ,ψ) plane: (a) $q=-0.7$ and (b) $q=-1$. The thick line in (a) shows the boundary l_b.

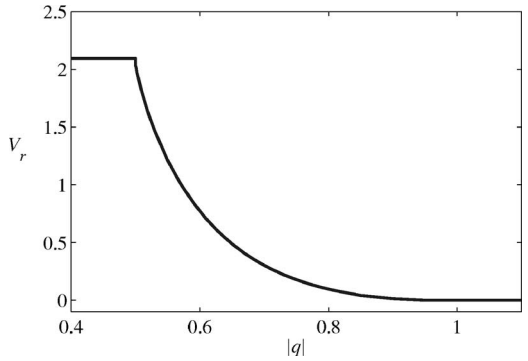

FIG. 5. The volume V_r of the regular domain as a function of $|q|$.

For $0.5<|q|<q_b$, the interior of the drop is divided between the regular domain and the chaotic domain. Numerically, we find $q_b\approx 0.96$ (see the Appendix for details). The regular domain corresponds to streamlines lying on the level sets of Φ that do not cross the separatrix [see Fig. 4(a)], whereas the rest of the streamlines belongs to the chaotic domain. As we explained earlier, the value of the AI can change significantly near the separatrix, leading to chaotic diffusion. This process is described in more detail in the next section. To leading order in ε, the boundary between the regular and the chaotic domain is a torus τ_b tangential to S. On the (φ,ψ) plane, τ_b corresponds to a closed curve l_b passing through the origin [see Fig. 4(a)]. Thus, we conclude that it is the level set $\Phi=\Phi(0,0)$ of the AI that serves as the boundary between the regular domain $[\Phi>\Phi(0,0)]$ and the chaotic domain $[\Phi<\Phi(0,0)]$. The computation of $\Phi(0,0)$ is outlined in the Appendix. Let us comment, however, that the level set $\Phi=\Phi(0,0)$ is not a sharp boundary: for any finite ε there are (although very few) regular trajectories inside the chaotic domain and vice versa. We will return to the discussion of the boundary between the domains in Sec. III E.

The AI reaches its minimum $(\Phi=0)$ on the outermost (almost square) trajectory, corresponding to the circle of the elliptic fixed points of the unperturbed system, and its maximum at an elliptic fixed point A of the averaged system where $\varphi=0$, $\psi=\psi_A(q,\beta)$. In the physical space, A corresponds to a stable periodic orbit l_A of the unperturbed system that resides in the $z=0$ plane. For $|q|>q_b$, the maximum of the AI always occurs at $\varphi=0$, $\psi=0$ (this point in the slow plane corresponds to the contours $\Gamma_{0^{\pm},0}$ in the physical space), so τ_b and l_b shrink to a point. As a result, all level sets of Φ intersect the separatrix and, consequently, all streamlines are chaotic. A typical phase portrait in this regime is shown in Fig. 4(b).

It follows from the description above that the volume V_r of the regular domain decreases in size from $2\pi/3$ (recall that we restricted our consideration to the hemisphere $y>0$) to 0 as $|q|$ increases from 0.5 to q_b (see Fig. 5).

D. Dynamics near the separatrix surface

As we have discussed earlier, some streamlines of the averaged system may cross the separatrix. Near the separatrix, the averaging procedure breaks down and, therefore, the value of Φ may change significantly. Our objective here is to calculate the change in Φ during a single passage of the exact system through the vicinity of S.

Consider a segment of a perturbed streamline that crosses the separatrix once and let M_I and M_F be the initial and final points of the segment lying at an $O(1)$ distance from the separatrix. Specifically, we consider the crossing from the $x>x_s$ to the $x<x_s$ part of the sphere (from $\psi<0$ to $\psi>0$). A reverse transition can be addressed in the same way. The problem is to calculate the change in the value of the AI, $\Delta\Phi=\Phi_F-\Phi_I$, over this segment for small ε.

It is shown in the Appendix that the jump of the AI is in the main approximation

$$\Delta\bar{\Phi}=\sqrt{\varepsilon}\bar{\Phi}(1-\bar{\Phi}^2)^{1/4}f(\xi), \tag{23}$$

where $f(\xi)$ describes the dependence of the jump magnitude on the distance between the crossing point and the axis, parameterized by variable ξ, $\bar{\Phi}=\Phi/\Phi(0,0)$ is the normalized value of the AI, and $\varphi_0=\cos^{-1}\bar{\Phi}$ defines the value of φ at which the crossing happens. The explicit definitions of ξ, $f(\xi)$, and $\Phi(0,0)$ are given in the Appendix. The values of ξ and $\bar{\Phi}$ (and hence $\Delta\bar{\Phi}$) can be calculated exactly for any initial condition (or choice of M_I). However, a small change of order ε in the initial conditions produces, in general, a large (order 1) change in ξ. Hence, for small ε it is possible to treat ξ as a random variable uniformly distributed on the unit interval.[12]

Equation (A22) was verified numerically for various values of parameters β, q, and ε. A typical plot of $f(\xi)$ is presented in Fig. 6. The function $f(\xi)$—and hence $\Delta\bar{\Phi}$—has singularities at both $\xi=0$ and $\xi=1$. Thus, there is a possibility (albeit quite small) of large changes in $\bar{\Phi}$ associated with a separatrix crossing. Using Eq. (A22), the ensemble average of $\Delta\bar{\Phi}$ can be shown to vanish regardless of the value of $\bar{\Phi}$:

$$\langle\Delta\bar{\Phi}\rangle=\int_0^1\Delta\bar{\Phi}(\xi,\bar{\Phi})d\xi=0. \tag{24}$$

E. Long term dynamics

In the present section we study the dynamics over long intervals of time that include many (of order $1/\varepsilon$) crossings of the separatrix. In the absence of molecular diffusion, mix-

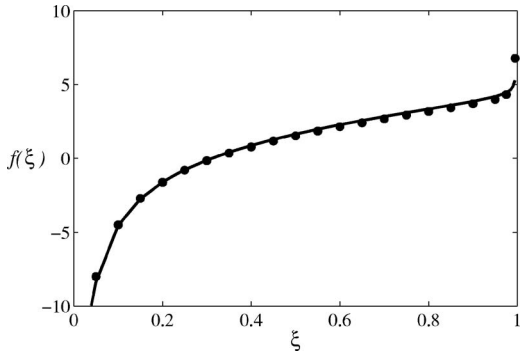

FIG. 6. The plot of $f(\xi)$ [see (23)] as a function of ξ. The solid line was obtained using the analytical result (A22) and the dots show the values obtained numerically from (4) for $\beta=0.5$, $q=-1$, $\varepsilon=10^{-3}$, and $\varphi_0=-\pi/3$.

ing inside the droplet is due solely to the chaotic advection, so the mixing properties of the flow are determined by its ergodicity. It has been shown elsewhere that in Hamiltonian and volume preserving systems, the accumulation of jumps of an AI at resonances or separatrices generically leads to chaotic advection and mixing (see, e.g., Refs. 11 and 13, and references therein). In particular, the existence of a positive Lyapunov exponent was shown in Ref. 14 and the ergodic properties in the limit of vanishing perturbation were discussed in Ref. 15.

Examples of typical dynamics in our system are presented in Fig. 7 as Poincaré sections of (4) by the $z=0$ plane for $q=-1$ (the top two rows) and for $q=-0.7$ (the bottom row). The left and the right panels in each row correspond to the same (typical) initial conditions but differ in the time of integration. One can see that the streamlines in the left panels of every row do not fill certain regions. For instance, the two

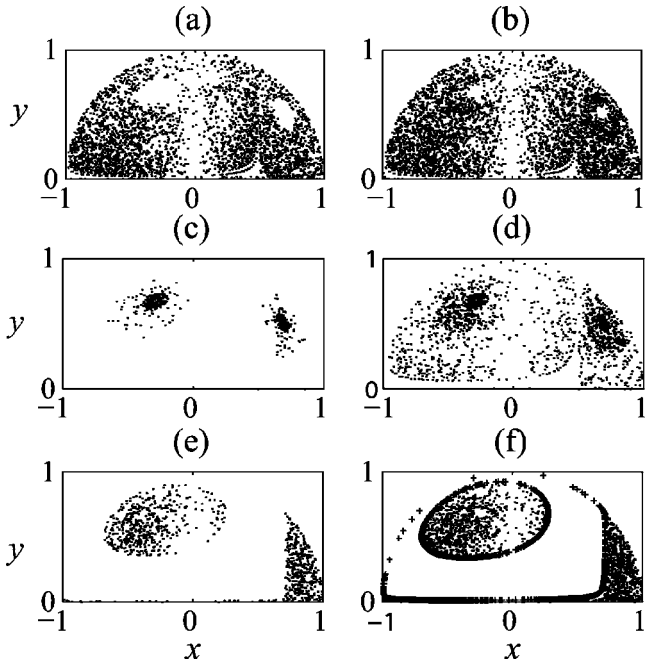

FIG. 7. Poincaré sections by the $z=0$ plane of a single streamline for $\varepsilon=10^{-3}$ and (a)–(d) $q=-1$, (e)–(f) $q=-0.7$. The integration time in the right column panels is twice that for the left column panels.

empty elliptic regions in Fig. 7(a) are inside the chaotic domain (the whole droplet is chaotic for $q=-1$) and correspond to neighborhoods of the elliptic fixed points where $\bar{\Phi}$ reaches an extremum; hence, $\Delta\bar{\Phi}$ vanishes. Therefore, it takes a long time for a streamline to "diffuse" there from a generic initial condition, although these regions are filled eventually as Fig. 7(b) demonstrates. For comparison, a streamline that starts near one of the circles of elliptic fixed points stays in their neighborhoods for a long time [Fig. 7(c)] before eventually escaping to cover the rest of the chaotic domain [Fig. 7(d)].

In contrast, the empty region in Fig. 7(e) forever remains empty. Indeed, for $q=-0.7$ the droplet interior is split between the regular and the chaotic domain. The empty region corresponds to the regular domain and a streamline that starts inside the chaotic domain never crosses its boundary τ_b [the bold symbols in Fig. 7(f) lie on the section of the torus τ_b by the Poincaré plane]. To avoid confusion, we note that the sparsely filled region around the $x=0$ plane in all six panels appears because $\dot{\varphi}=0$ on the plane [see (10)]. Consequently, the streamlines are oriented locally parallel to the Poincaré plane $z=0$ instead of intersecting it.

These examples suggest that two different (and generally unrelated) metrics should be used to describe chaotic advection in a bounded flow such as the one considered here: the size of the chaotic domain and the characteristic rate of mixing inside the chaotic domain.

The first of these two metrics, the volume V_c of the chaotic domain (that is related to the volume V_r of the regular domain by a trivial relation $V_c+V_r=2\pi/3$), is found to depend on q but not on ε (for infinitesimal ε). As we have already determined (see Fig. 5), depending on the value of q, the interior of the drop can be completely regular (for $|q|<0.5$), partially regular, and partially chaotic (for $0.5<|q|<q_b$), or completely chaotic (for $|q|>q_b$). The size of the chaotic domain is, to leading order, determined by the shape of its boundary—the torus τ_b—which is independent of ε. However, for any finite ε, the boundary between the two domains is more complex. The chaotic domain penetrates inside τ_b adding a layer with thickness of order $\sqrt{\varepsilon}$ (see Ref. 16 for details). Further, small islands of stability appear inside this layer [see, e.g., Fig. 1(c)]. As a result there is an $O(\sqrt{\varepsilon})$ correction to V_c.

Recall that for $\varepsilon=0$, the whole interior is completely regular regardless of the value of q (see Sec. III A). The chaotic domain of a finite size $V_c(q)$ appears as soon as ε becomes nonzero. This is due to the fact that, while the separatrix crossing events themselves are local (they are governed only by the dynamics in the vicinity of a separatrix surface, which is ε dependent), their effect is global, extending the chaotic domain to the scale of the entire drop.

We have verified numerically that inside the chaotic domain one does indeed find a positive Lyapunov exponent for $\varepsilon>0$, confirming the divergence of nearby streamlines. Furthermore, for small ε, the flow possesses good ergodic properties inside the mixing domain, as the Poincaré sections presented in Fig. 7 illustrate, indicating very thorough mixing. Indeed, the chaotic domain is essentially devoid of regular islands, so a single streamline densely fills the whole

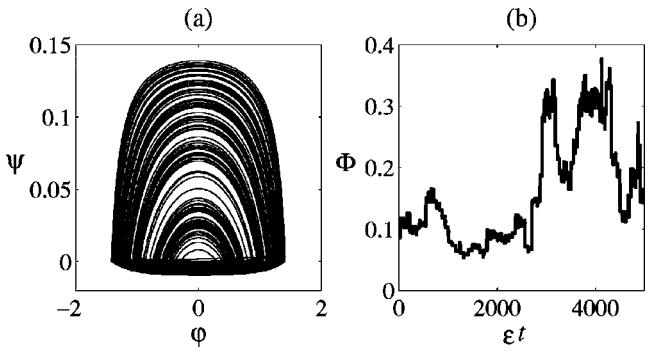

FIG. 8. A typical chaotic streamline for $q=-1$ and $\varepsilon=10^{-3}$ computed over a long time period: (a) Projection onto the (φ,ψ) plane, (b) evolution of the AI.

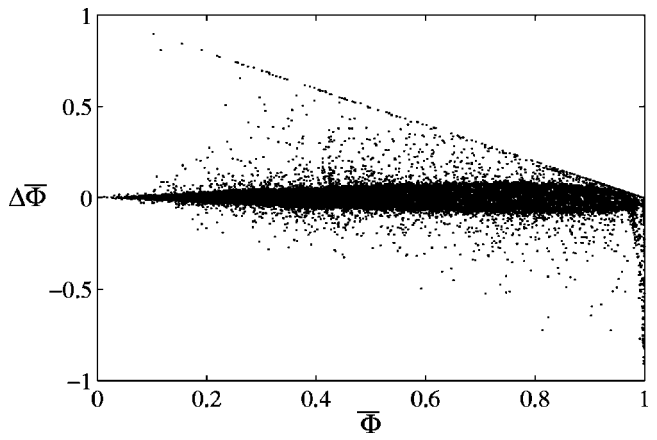

FIG. 9. The distribution of the sizes of the jumps $\Delta\bar{\Phi}$ versus the values of $\bar{\Phi}$ before the crossings.

chaotic domain. (The sparsely populated vertical strip in the middle merely reflects the fact that, at $x=0$, the streamlines are tangential to the Poincaré plane $z=0$.) For decreasing ε, the regular islands (of size $\sqrt{\varepsilon}$) are expected to gradually disappear, resulting in perfect mixing.

The second metric, the rate of mixing D, on the other hand, strongly depends on ε. Indeed, consider the evolution from a typical initial condition for $|q|>q_b$. Figures 8(a) and 8(b) show the projection of one such streamline onto the slow plane and the evolution of the AI, respectively. One can see that the streamline densely covers the domain with Φ ranging almost from its minimum $\bar{\Phi}=0$ to its maximum $\bar{\Phi}=1$ (i.e., essentially the whole interior of the droplet). Once again, it takes a very long time for the streamline to diffuse near either of the extrema of $\bar{\Phi}$, since $\Delta\bar{\Phi}$ vanishes there.

The rate of mixing inside the chaotic domain can be computed using the statistics of changes in the AI. As the average change in $\bar{\Phi}$ at a separatrix crossing is zero, one should expect $\bar{\Phi}$ to evolve diffusively over long times. Quantitative properties of the diffusion of the AI depend on whether consecutive crossings are statistically dependent or independent. In volume-preserving systems, statistical independence can be deduced from the divergence of phases ξ along streamlines. A similar problem for the Hamiltonian system was discussed in Ref. 17.

Assuming statistical independence of consecutive crossings, we can describe the evolution of $\bar{\Phi}$ by a random walk with a characteristic step size of order $\sqrt{\varepsilon}$. Hence, after N crossings, the value of $\bar{\Phi}$ changes by a quantity of order $\sqrt{N}\times\sqrt{\varepsilon}$. The mixing can be considered complete when a typical chaotic streamline samples the entire chaotic domain. The difference between the values of Φ that bound the chaotic domain in our problem is of order unity. Therefore, it takes on the order of $N\sim 1/\varepsilon$ separatrix crossings for diffusion to cover the whole domain. As the typical time between successive crossings is of order $1/\varepsilon$, we find the characteristic time for mixing to be $T_M=O(\varepsilon^{-2})$. This characteristic time diverges for $\varepsilon\to 0$, so the rate of mixing, defined as $D=1/T_M=O(\varepsilon^2)$, vanishes for $\varepsilon\to 0$. We, therefore, recover the result that, for $\varepsilon=0$, the dynamics becomes completely regular for all q.

In the conclusion of this section, we briefly mention that in the limit of an infinitely viscous droplet (i.e., for $\beta=0$), the magnitude of the jump is reduced to $\Delta\bar{\Phi}=O(\varepsilon\ln\varepsilon)$ (see the Appendix for details), resulting in a drastic decrease of the mixing rate to $D=1/T_M=O(\varepsilon^3(\ln\varepsilon)^2)$. The value of β has no effect on the size of the mixing domain.

F. Finite perturbations

In most of the previous perturbative studies of chaotic diffusion, only infinitesimal perturbations were considered. To the best of our knowledge, the only paper that addresses, in any significant detail, the case of finite ε is Ref. 18.

The dynamics of our system in the presence of a small but finite perturbation differs in several important ways from that with an infinitesimally small perturbation. First, the very applicability of the method of averaging for larger ε is somewhat questionable, as the ratio of the characteristic frequencies [e.g., $\Omega(\psi)$ and ε in (14)] may not be very large. Numerical simulations, however, indicate that the major result of the averaging method, that $\bar{\Phi}$ still changes most significantly near the separatrix, holds for a wide range of ε.

The second effect is that for finite values of ε there is a finite probability that the jump size can become comparable to the range of the AI [e.g., $\bar{\Phi}\in(0,1)$ for $|q|>q_b$]. Consequently, the boundaries of the system start playing an important role in the statistics of the jumps. While magnitudes of most of the jumps are still given by (A22) and satisfy the zero-average statement, the distribution of large jumps differs from the original prediction. Indeed, (A22) breaks down when the value of $\bar{\Phi}$ either before or after the separatrix crossing is close to one of the domain boundaries. Take, for example, $\varepsilon=10^{-3}$ and $q=-1$. Then, approximately 0.1% of the jumps feel the presence of the boundaries. While the influence of the boundaries on the properties and statistics of single crossings (albeit for a different system) was discussed in detail in Ref. 18, here we are interested in necessary modifications to the long-time dynamics of the system and, in particular, the rate of mixing.

Figure 9 presents the distribution of the sizes of the jumps $\Delta\bar{\Phi}$ versus the values of $\bar{\Phi}$ before the corresponding

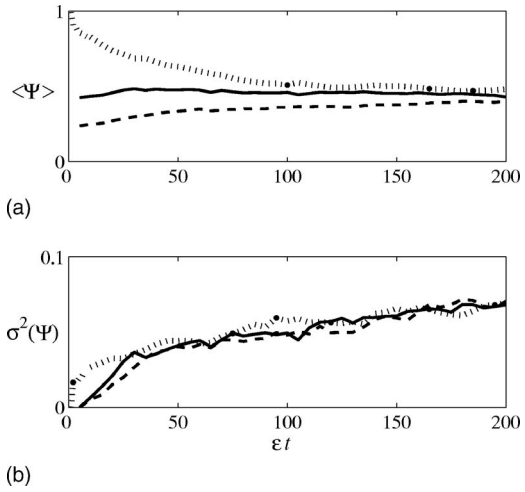

FIG. 10. Time evolution of (a) $\langle\Psi\rangle$, (b) $\sigma^2(\Psi)$.

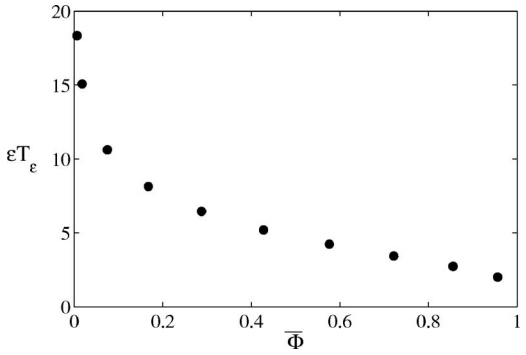

FIG. 11. The normalized slow period, $\varepsilon T_\varepsilon$, for several characteristic values of $\bar{\Phi}$; $q=-1$.

crossing. There are three types of jumps. Most of the jumps are small and concentrate near the $\bar{\Phi}$ axis (the densely covered region). These jumps are well described by (23) and (A22). In particular, the average value of these jumps is zero. The second type are jumps corresponding to points that lie between the lines $\bar{\Phi}_{n+1}=\bar{\Phi}_n+\Delta\bar{\Phi}_n=\pm 1$, but outside of the densely covered region. These jumps happen when streamlines pass through the vicinities of the singularities of $\Delta\bar{\Phi}(\xi)$, given by (A22). Such jumps were studied in detail in Ref. 18. Finally, there are jumps that lie on either of the lines $\bar{\Phi}_{n+1}=\bar{\Phi}_n+\Delta\bar{\Phi}_n=1$ and $\bar{\Phi}_n=1$. They were called "axis crossings" in Ref. 19.

Denoted by $\Psi=\Psi(\bar{\Phi},t)$ a probability density function (PDF) of the values of the AI at time t for an ensemble of streamlines. To check the long-time evolution of such PDFs, we integrated three ensembles, each composed of 240 streamlines, with initial conditions localized in different parts of the phase space: in the vicinity of the elliptic fixed points (the smallest values of $\bar{\Phi}$), in the midrange of $\bar{\Phi}$, and near the surface of the sphere (the largest values of $\bar{\Phi}$).

One can see in Fig. 10(a) a definite drift of the ensemble average $\langle\Psi\rangle$ of the AI for each of the three ensembles, a manifestation of a nonzero jump average $\langle\Delta\Phi\rangle$. This drift is, of course, quite natural: the asymptotic distribution inside the chaotic domain is expected to be independent of the initial distribution. Without going into detail, let us comment that numerical simulations show that it is the large jumps of Φ that cause the drift.

On the other hand, aggregate changes due to smaller jumps result in the spreading of the PDF [see Fig. 10(b)]. The linear growth of the dispersion $\sigma^2(\Psi)$ at small times indicates a classical random walk in an unbounded domain; initially, most of the streamlines are relatively far away from the boundaries. Different slopes reflect not only the dependence of the average jump magnitude on $\bar{\Phi}$ but also the difference in periods of the slow system for the three ensembles—larger values of $\bar{\Phi}$ correspond to more frequent separatrix crossings. The period $T_\varepsilon(\bar{\Phi})$ has a minimum at $\bar{\Phi}=1$ and blows up logarithmically at $\bar{\Phi}=0$ (see Fig. 11). However, after a certain time, the difference between the average values of $\bar{\Phi}$ [and, hence, between the values of $T_\varepsilon(\bar{\Phi})$] decreases and the slope of $\sigma^2(\Psi)$ settles to a common value defined by a random walk in a domain with boundaries.

The above considerations describe diffusion in an ensemble of streamlines *across* the level sets of the AI. Mixing *within* the toroidal level sets of the AI would typically occur faster. The stretching in the direction along the coils of the unperturbed system is due to the variation in $\Omega(\psi)$, while the stretching in the direction normal to the coils of the unperturbed system is due to variation of $T_\varepsilon(\bar{\Phi})$. For an ensemble of streamlines originating inside a sphere of radius δ, the corresponding time scales of homogenization will be, respectively, $O(\varepsilon^{-2})$, $O(\delta^{-1})$, and $O(\varepsilon^{-1}\delta^{-1})$. For $\varepsilon \ll \delta$, it is the longest time scale $T_M=O(\varepsilon^{-2})$ that determines how quickly the mixing in 3D occurs.

IV. DISCUSSION AND FUTURE TOPICS

In this paper we considered mixing via chaotic advection in thermocapillary driven droplets in the limit of vanishing molecular diffusion. Efficient mixing in experiment usually means that the flow quickly homogenizes the distribution of the advected physical entity (e.g., temperature or concentration) such that, eventually, the distribution becomes uniform (or nearly so) over a large fraction of the total volume. For instance, if the asymptotic distribution is uniform, but the mixing rate is very small, on the experimental time scale only highly nonuniform distributions can be realized. A similar outcome will result for a flow with a large mixing rate and a small relative volume of the chaotic domain.

As we have shown, these two metrics, the mixing rate and the mixed volume fraction, are essentially independent and are controlled by different physical mechanisms. In this particular physical realization of the flow, the mixing rate increases when the temperature coefficient of surface tension at the substrate top surface increases relative to that at the droplet surface (parameter ε above).

The volume fraction, on the other hand, depends on both ε and the degree of nonuniformity of the temperature gradient (parameter q above). The mixed volume fraction in-

creases with the curvature of the temperature field, covering the whole droplet interior for $|q| \gtrsim 0.96$ for small ε. At smaller curvatures (e.g., $|q| < 0.5$), the flow only homogenizes the distribution over 2D shells rather than in 3D (zero mixed volume fraction), so that advection becomes a very inefficient mixing mechanism.

The mixing properties of the flow also deteriorate with increasing ε. According to numerical simulations, for $\varepsilon \gtrsim |q|$, the mixed volume fraction decreases almost to zero, as the chaotic domain shrinks around a streamline connecting a pair of fixed points in the symmetry plane $y=0$. In this case the mixing occurs effectively in 1D instead of 3D. A detailed study of finite ε will be reported in a separate publication.

We have not included the explicit dependence of the dipole and quadrupole components of the flow on the parameter β describing the relative viscosities. When the droplet becomes much more viscous than the substrate fluid (i.e., in the limit $\beta \to 0$), both the dipole and the quadrupole component become strongly suppressed $[v_d = O(\beta),\ v_q = O(\beta)]$ and can be ignored (see Ref. 6 for details). In this limit, the flow described by the Taylor component alone becomes integrable and one again finds mixing to effectively occur in 1D.

Another topic that deserves a separate discussion is a quantitative description of the evolution of probability distribution functions for finite values of ε. In particular, to the best of our knowledge, the properties of the asymptotic distribution (e.g., uniformity over the chaotic domain) were never studied in great detail. We plan to address the evolution of PDFs in a subsequent publication.

Summing up, the best (in terms of both speed and thoroughness) mixing is expected to be found in the flows where (a) the viscosity of the droplet is smaller than, or similar to, that of the substrate fluid, (b) the temperature field has significant curvature (on the scale of the droplet diameter), and (c) the temperature coefficients of surface tension at the two interfaces have similar magnitudes. Conditions (a) and (c) are fairly typical and will be easy to enforce in an experiment, such as the one reported in Ref. 7. Condition (b) is the most challenging, especially for small droplets (e.g., tens of microns).

ACKNOWLEDGMENTS

This material is based upon work supported by the National Science Foundation under Grant No. 0400370. Acknowledgment is also made to the Donors of the American Chemical Society Petroleum Research Fund, for partial support of this research. D.L.V. is grateful to the Russian Basic Research Foundation Grant No. 06-01-00117. We are grateful for useful discussions with A. I. Neishtadt and A. A. Vasiliev.

APPENDIX: JUMP OF THE ADIABATIC INVARIANT

An expression for the jump of the AI upon one crossing of the separatrix plane can be derived by expanding Φ in the vicinity of S (i.e., for small $|\psi|$). At the leading order

$$\Phi(\psi,\varphi) = \Phi^{(0)}(\varphi) + \Phi^{(1)}_{\pm}(\psi,\varphi) + O(\psi \ln|\psi|) \tag{A1}$$

(see Ref. 11 for the error estimates and a more detailed discussion of this expansion). Here $\Phi^{(0)}(\varphi)$ is a flux through one of the separatrix contours $\Gamma_{0^{\pm},\varphi}$. For $q < -0.5$, the contour $\Gamma_{0^{+},\varphi}$ corresponding to the streamline with $\psi \to 0^{+}$ consists of a segment of the x axis from $x=-1$ to $x=x_s$, a line on the separatrix between the x axis and the surface of the drop, and an arc on the surface closing the contour. Similarly, the contour $\Gamma_{0^{-},\varphi}$ corresponding to the streamline with $\psi \to 0^{-}$ includes a part of the x-axis from $x=1$ to $x=x_s$, a line on the separatrix between the x axis and the surface of the drop, and an arc on the surface closing the contour. Each of these two contours connects three different hyperbolic fixed points. Only the segment of the contour lying in the separatrix plane contributes to the integral in (19):

$$\begin{aligned}\Phi^{(0)}(\varphi) &= \cos\varphi \int_0^1 (1 - x_s^2 - \rho^2)(\beta x_s^2 - 1) d\rho \\ &= \tfrac{2}{3}(1 - \beta x_s^2)(1 - x_s^2)^{3/2} \cos\varphi,\end{aligned} \tag{A2}$$

so the value of $\Phi^{(0)}(\varphi)$ is the same for $\Gamma_{0^{-},\varphi}$ and $\Gamma_{0^{+},\varphi}$. The next order correction terms correspond to the flux through a narrow strip between $\Gamma_{0^{\pm},\varphi}$ and $\Gamma_{\psi,\varphi}$, which vanishes as $\psi \to 0$:

$$\Phi^{(1)}_{\pm}(\psi,\varphi) = 2a_{\pm}(\varphi,\beta)\sqrt{|\psi|}, \tag{A3}$$

where

$$\begin{aligned}a_{-}(\varphi,\beta) &= -\frac{\beta}{\sqrt{2}} \cos\varphi \int_1^{x_s} \frac{x(5x^2-7)}{\sqrt{|1+2qx|(1-x^2)}} dx, \\ a_{+}(\varphi,\beta) &= -\frac{\beta}{\sqrt{2}} \cos\varphi \int_{-1}^{x_s} \frac{x(5x^2-7)}{\sqrt{(1+2qx)(1-x^2)}} dx.\end{aligned} \tag{A4}$$

The subscripts of $\Phi^{(1)}$ and a coincide with the sign of ψ and indicate what side of the separatrix the streamline of the unperturbed system lies on. Unlike most cases reported in the literature (see, e.g., Ref. 11), the values of a_{-} and a_{+} are different.

Using expansion (A1), we can find the value of q at which the regular domain disappears in the limit of $\varepsilon \to 0$. Since $\dot{\varphi} = \dot{\psi} = 0$ at A, it follows from (15) and (18) that the value of q_b is given by

$$\int_{-1}^{x_{s,b}} \frac{x(5x^2-7)}{\sqrt{(1+2q_b x)(1-x^2)}} dx = 0, \tag{A5}$$

where $x_{s,b} = -1/(2q_b)$. Solving this equation numerically we find $q_b \approx 0.96$.

Far from the separatrix the streamline of the exact system lies (almost) on a toroidal level set surface of $\Phi(\psi,\varphi)$. Recall that the variable s is fast while ψ and φ are slow, so for any nonzero ε almost all the streamlines do not close [after the period $T(\psi)$] and instead revolve around the torus, resembling a spiral (see Fig. 3) with every coil being near a closed streamline of the unperturbed system with the same values of ψ and φ. On each turn of the spiral between M_I and M_F we mark the point closest to the surface of the sphere

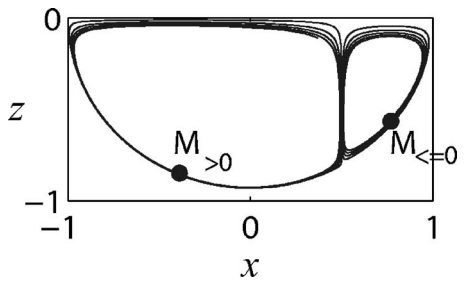

FIG. 12. The projection of a typical streamline near the separatrix on the (x,z) plane. The parameters are $\varepsilon=10^{-3}$, $q=-1$.

(where $s=0$ for the unperturbed system). If we denote these points M_k and enumerate them in such a way that $k\leqslant 0$ before the crossing (for $\psi<0$ under our assumptions) and $k>0$ after the crossing (for $\psi>0$), then increasing $|k|$ corresponds to receding from the separatrix. Thus, M_0 is the last of the points M_k prior to the separatrix crossing, and M_1 is the first of those after the crossing. The turn of the streamline between M_{k-1} and M_k is called the kth turn and is denoted by γ_k. A few turns of a typical streamline in the immediate vicinity of S are shown in Fig. 12. Each turn γ_k can be divided into three parts: the one near the x axis, the one near the separatrix plane, and the one near the surface of the sphere.

Let ψ_k, φ_k, and Φ_k be the values of the functions ψ, φ, and Φ at the point M_k. We now evaluate the changes in these functions on the kth turn of the streamline. For the change in ψ we have

$$\psi_k-\psi_{k-1}=\int_{\gamma_k}\frac{d\psi}{dt}dt. \tag{A6}$$

One finds that the main contribution to this integral comes from the part of γ_k close to the plane $x=x_s$. Indeed, the second term in the first line of (13) almost vanishes at each of the three segments of the turn, while the first term almost vanishes near the x axis and near the surface of the sphere. We replace γ_k in (A6) by $\Gamma_{0,\varphi}$ and, estimating the error introduced as a result of this, we find

$$\psi_k-\psi_{k-1}=\varepsilon\Theta_k+O(\varepsilon\sqrt{|\psi_{k-1}|})+O(\varepsilon^2\ln|\psi_k|), \tag{A7}$$

where we have defined

$$\Theta_k=-\tfrac{2}{3}(1-\beta x_s^2)(1-x_s^2)^{3/2}\sin\varphi_k. \tag{A8}$$

One can see that the transition from $x>x_s$ to $x<x_s$ occurs where $\sin\varphi<0$. Note that (A7) is valid on either side of the separatrix, i.e., before and after crossing.

Analogously, the main contribution to the change in φ is given by the part of γ_k near the x axis, where ρ is small:

$$\varphi_k-\varphi_{k-1}=-\varepsilon a_{k-1}\frac{\operatorname{sign}(\psi_{k-1})}{\sqrt{|\psi_{k-1}|}}+O(\varepsilon\ln|\psi_k|)+O(\varepsilon^2|\psi_{k-1}|^{-1}), \tag{A9}$$

where

$$\begin{aligned}a_{k-1}&=a_-(\varphi_{k-1},\beta),\quad k\leqslant 1,\\ a_{k-1}&=a_+(\varphi_{k-1},\beta),\quad k>1,\end{aligned} \tag{A10}$$

and $a_\pm$ were defined in (A4). The estimates of the residual terms in (A7) and (A9) were made under the assumption that $C\varepsilon^{3/2}<|\psi_0|<\varepsilon\Theta_0-C\varepsilon^{3/2}$, $C=\text{const}>0$.

One can see that to leading order

$$\Delta\varphi=-\varepsilon\frac{\partial\Phi}{\partial\psi}\approx-\varepsilon\frac{\partial\Phi^{(1)}}{\partial\psi},\quad \Delta\psi\approx\varepsilon\frac{\partial\Phi^{(0)}}{\partial\varphi}. \tag{A11}$$

Therefore, using (A7) and (A9), and expression for the AI (A1), we find the change of Φ along γ_k to be

$$\begin{aligned}\Phi_k-\Phi_{k-1}=&-a_{k-1}\varepsilon\Theta_k\frac{\operatorname{sign}(\psi_{k-1})}{\sqrt{|\psi_{k-1}|}}\\ &+2(a_k\sqrt{|\psi_k|}-a_{k-1}\sqrt{|\psi_{k-1}|})\\ &+O(\varepsilon^2(|\psi_{k-1}|^{-1}+|\psi_k|^{-1})).\end{aligned} \tag{A12}$$

The estimate of the residual term in (A12) follows from the definition of an AI (see, e.g. Ref. 14), as the change in Φ over a turn of the spiral well away from the separatrix [at an $O(1)$ distance] is of order ε^2. Thus, the aggregated change in Φ on all $(\sim 1/\varepsilon)$ coils away from the separatrix is of order ε. Consequently, any larger than order ε contribution to the total change in Φ can only come from the turns passing near the separatrix. Therefore, the total change in the AI over a long segment of a streamline crossing the separatrix is dominated by the contribution from the turns near the separatrix and can be computed by summing up contributions (A12):

$$\begin{aligned}\Delta\Phi=&\sum_{k=-N^-+1}^{N^+}\left[-a_{k-1}\varepsilon\Theta_k\frac{\operatorname{sign}(\psi_{k-1})}{\sqrt{|\psi_{k-1}|}}\right.\\ &\left.+2(a_k\sqrt{|\psi_k|}-a_{k-1}\sqrt{|\psi_{k-1}|})\right]+O(\varepsilon|\ln\varepsilon|)\\ &+O(\varepsilon^2(|\psi_0|^{-1}+|\psi_1|^{-1})),\end{aligned} \tag{A13}$$

where N^- and N^+ are integers of order $1/\varepsilon$. The leading term in $\Delta\Phi$ does not depend on the exact choice of $N^\pm$ (in the majority of corresponding numerical simulations the series converges for much smaller values of $N^\pm$). Furthermore, all the terms in the parentheses in (A13) cancel out except for the two end terms.

To simplify (A13), note that during the motion on the turns just before or after the separatrix the value of φ does not change much; a change in φ is small, while characteristic values of φ are $O(1)$. Therefore, to leading order we can set $\varphi_k\approx\varphi_0$, so that

$$\Theta_k\approx\Theta_0\quad\text{and}\quad\psi_k\approx\psi_0+k\varepsilon\Theta_0. \tag{A14}$$

Similarly, we have

$$\begin{aligned}a_{k-1}&=a_-(\varphi_0,\beta),\quad k\leqslant 1,\\ a_{k-1}&=a_+(\varphi_0,\beta),\quad k>1.\end{aligned} \tag{A15}$$

Substituting the above expressions into (A13), we get

$$\Delta\Phi = \sum_{k=-N^-+1}^{N^+} \left[-a_{k-1}\varepsilon\Theta_0 \frac{\mathrm{sign}(\psi_0+(k-1)\varepsilon\Theta_0)}{\sqrt{|\psi_0+(k-1)\varepsilon\Theta_0|}} \right] + 2(a_k|\psi_0+N^+\varepsilon\Theta_0|^{1/2} - a_{k-1}|\psi_0+N^-\varepsilon\Theta_0|^{1/2}) + O(\varepsilon|\ln\varepsilon|) + O(\varepsilon^2(|\psi_0|^{-1}+|\psi_1|^{-1})). \quad \text{(A16)}$$

Introduce a dimensionless variable $\xi=-\psi_0/(\varepsilon\Theta_0)$, $\xi\in(0,1)$ characterizing how far from the axis the streamline crosses the separatrix plane. With this definition we obtain

$$\Delta\Phi = \sqrt{\varepsilon|\Theta_0|}\left(\sum_{k=0}^{N^--1} \frac{a_-}{\sqrt{\xi+k}} - \sum_{k=0}^{N^+-1} \frac{a_+}{\sqrt{-\xi+1+k}} \right) + 2\sqrt{\varepsilon|\Theta_0|}(a_+(-\xi+N^+)^{1/2} - a_-(\xi+N^-)^{1/2}) + \mathrm{Err}, \quad \text{(A17)}$$

where

$$\mathrm{Err} = O(\varepsilon|\ln\varepsilon|) + \varepsilon O(\xi^{-1}+(1-\xi)^{-1}) \quad \text{(A18)}$$

is the error term. Using a definition of the gamma function,[20]

$$\Gamma\left(\frac{1}{2}\right) = \sqrt{\pi} = p^{1/2}\int_0^\infty t^{-1/2}e^{-pt}dt, \quad p>0, \quad \text{(A19)}$$

and following Refs. 11 and 16, the sum in (A17) can be expressed in the form of an integral. We arrive at

$$\Delta\Phi = \frac{\sqrt{\varepsilon|\Theta_0|}}{\sqrt{\pi}}\left(a_-\int_0^\infty \frac{1}{\sqrt{t}}\frac{e^{-\xi t}-e^{-t}}{1-e^{-t}}dt - a_+\int_0^\infty \frac{1}{\sqrt{t}}\frac{e^{-(1-\xi)t}-e^{-t}}{1-e^{-t}}dt + (a_-J^-_{1/2}(N^-) - a_+J^+_{1/2}(N^+)) \right) + \mathrm{Err}, \quad \text{(A20)}$$

where

$$J^\pm_{1/2}(N^\pm) = \int_0^\infty \frac{1}{\sqrt{t}}\frac{e^{-t}-e^{-N^\pm t}}{1-e^{-t}}dt - 2\sqrt{\pi}\sqrt{N^\pm}. \quad \text{(A21)}$$

Taking the limit $N^\pm\to\infty$, we finally obtain

$$\Delta\Phi = \frac{\sqrt{\varepsilon|\Theta_0|}}{\sqrt{\pi}}\left(a_-\int_0^\infty \frac{1}{\sqrt{t}}\frac{e^{-\xi t}-e^{-t}}{1-e^{-t}}dt - a_+\int_0^\infty \frac{1}{\sqrt{t}}\frac{e^{-(1-\xi)t}-e^{-t}}{1-e^{-t}}dt + (a_- - a_+)J_{1/2} \right) + \mathrm{Err}, \quad \text{(A22)}$$

where

$$J_{1/2} = \lim_{N^\pm\to\infty} J^\pm_{1/2}(N^\pm) \approx -2.5884. \quad \text{(A23)}$$

Using (A2), we can express $\cos\varphi_0$ in terms of the value of Φ at M_0:

$$\cos\varphi_0 = \Phi/\Phi(0,0) \equiv \bar{\Phi}, \quad \text{(A24)}$$

where, according to (A1) and (A2),

$$\Phi(0,0) = \tfrac{2}{3}(1-\beta x_s^2)(1-x_s^2)^{3/2}. \quad \text{(A25)}$$

Moreover, as characteristic values of $\Delta\Phi$ at a single crossing are small (it is the accumulation of those changes that leads to mixing), the value of Φ at an initial conditions far from the separatrix can be used in (A22) and (A24). Substituting (A24) into the definitions of Θ_0 and $a_\pm$ and further into (A22), we obtain the "separatrix map" that relates the values of the AI before and after the crossing,

$$\Delta\bar{\Phi} = \sqrt{\varepsilon}\bar{\Phi}(1-\bar{\Phi}^2)^{1/4}f(\xi), \quad \text{(A26)}$$

where $f(\xi)$ describes the dependence of the jump magnitude on the distance between the crossing point and the axis. The integrals defining $f(\xi)$ diverge for both $\xi\to0^+$ and $\xi\to1^-$, so (A22) is accurate only for $C\sqrt{\varepsilon}<\xi<1-C\sqrt{\varepsilon}$, with some $C=\mathrm{const}>0$.

In the limit of an infinitely viscous droplet (i.e., for $\beta=0$ or $\lambda=\infty$), the value of Θ_0 remains finite [see (A8)], but $a_\pm$ vanishes. Therefore, the leading order term given in (A22) vanishes. By including the next term in (A1) one can show that the magnitude of the jump is reduced to $\Delta\Phi=O(\varepsilon\ln\varepsilon)$ (see Ref. 11). In fact, as far as the qualitative dependence of the jumps of the AI on ε is concerned, the system with $\beta=0$ is closer to a time-dependent 2D flow (see, e.g., Ref. 21) than to a generic steady 3D flow, such as the one considered in the present paper.

Finally, let us remark that if the dipole flow is much weaker than the quadrupole flow (i.e., for $q\to\infty$), the separatrix coincides with the equator plane $x_s=0$. Hence, $a_+=a_-$, the term with $J_{1/2}$ in (A22) vanishes, and we obtain an expression for the jump similar to Eq. (23) from Ref. 11.

[1] R. F. Ismagilov, J. M. K. Ng, P. J. A. Kenis, and G. M. Whitesides, "Microfluidic arrays of fluid-fluid diffusional contacts as detection elements and combinatorial tools," Anal. Chem. **73**, 5207 (2001).
[2] H. A. Stone and Z. B. Stone, "Imaging and quantifying mixing in a model droplet micromixer," Phys. Fluids **17**, 063103 (2005).
[3] M. Muradoglu and H. A. Stone, "Mixing in a drop moving through a serpentine channel: A computational study," Phys. Fluids **17**, 073305 (2005).
[4] T. Ward and G. M. Homsy, "Electrohydrodynamically driven chaotic mixing in a translating drop," Phys. Fluids **13**, 3521 (2001).
[5] T. Ward and G. M. Homsy, "Electrohydrodynamically driven chaotic mixing in a translating drop. II. Experiments," Phys. Fluids **15**, 2987 (2003).
[6] R. O. Grigoriev, "Chaotic mixing in thermocapillary-driven microdroplets," Phys. Fluids **17**, 033601 (2005).
[7] R. O. Grigoriev and M. F. Schatz, "Optically controlled mixing in microdroplets," Lab Chip **6**, 1369 (2006).
[8] V. I. Arnold, V. V. Kozlov, and A. I. Neishtadt, *Dynamical Systems III. Encyclopedia of Mathematical Sciences* (Springer-Verlag, New York, 1988).
[9] N. N. Bogolyubov and Yu. A. Mitropolsky, *Asymptotic Methods in the Theory of Nonlinear Oscillations* (Gordon and Breach, New York, 1961), Vol. 537.
[10] V. I. Arnold, *Geometrical Methods in the Theory of Ordinary Differential Equations* (Springer-Verlag, New York, 1983).
[11] A. I. Neishtadt, D. L. Vainshtein, and A. A. Vasiliev, "Chaotic advection in a cubic Stokes flow," Physica D **111**, 227 (1998).
[12] A. I. Neishtadt, "On adiabatic invariance in two-frequency systems," in *Hamiltonian Systems With 3 or More Degrees of Freedom*, NATO ASI Series C (Kluwer, Dordrecht, 1999), Vol. 533, pp. 193–213.

[13]D. L. Vainchtein, A. I. Neishtadt, and I. Mezic, "On passage through resonances in volume-preserving systems," Chaos **16**, 043123 (2006).
[14]D. L. Vainshtein, A. A. Vasiliev, and A. I. Neishtadt, "Changes in the adiabatic invariant and streamline chaos in confined incompressible Stokes flow," Chaos **6**, 67 (1996).
[15]A. I. Neishtadt and A. A. Vasiliev, "Change of the adiabatic invariant at a separatrix in a volume-preserving 3D system," Nonlinearity **12**, 303 (1999).
[16]D. L. Vainshtein, A. A. Vasiliev, and A. I. Neishtadt, "Adiabatic chaos in a two-dimensional mapping," Chaos **6**, 514 (1996).
[17]A. I. Neishtadt and A. A. Vasiliev, "Phase change between separatrix crossings in slow-fast Hamiltonian systems," Nonlinearity **18**, 1393 (2005).
[18]A. I. Neishtadt, C. Simo, and A. A. Vasiliev, "Geometric and statistical properties induced by separatrix crossings in volume-preserving systems," Nonlinearity **16**, 521 (2003).
[19]D. Kroujiline and H. A. Stone, "Chaotic streamlines in steady bounded three-dimensional Stokes flows," Physica D **130**, 105 (1999).
[20]L. S. Gradshtein and I. M. Ryzhik, *Tables of Sums, Integrals and Series* (Academic, Boston, 1994).
[21]A. I. Neishtadt, "Change of an adiabatic invariant at a separatrix," Sov. J. Plasma Phys. **12**, 568 (1986).